ESC European Society of Cardiology

European Heart Journal - Cardiovascular Imaging (2017) **18**, 1253–1261
doi:10.1093/ehjci/jew222

Quantitative intravascular biological fluorescence-ultrasound imaging of coronary and peripheral arteries *in vivo*

Dmitry Bozhko[1†], Eric A. Osborn[2,3†], Amir Rosenthal[1], Johan W. Verjans[2], Tetsuya Hara[2], Stephan Kellnberger[1,2], Georg Wissmeyer[1], Saak V. Ovsepian[1], Jason R. McCarthy[2], Adam Mauskapf[2], Ashley F. Stein[2], Farouc A. Jaffer[2*‡], and Vasilis Ntziachristos[1‡]

[1]Helmholtz Zentrum München, Institute for Biological and Medical Imaging, Ingolstädter Landstr. 1, 85764, Neuherberg, Germany; Chair for Biological Imaging (CBI), Technische Universität München (TUM), Trogerstr. 9, 81675, Munich, Germany; [2]Cardiovascular Research Center and Cardiology Division, Massachusetts General Hospital, Harvard Medical School, 185 Cambridge Street, Boston, MA 025114, USA; and [3]Cardiology Division, Beth Israel Deaconess Medical Center, Harvard Medical School, 330 Brookline Avenue, Boston, MA 02215, USA

Received 18 May 2016; accepted after revision 2 October 2016; online publish-ahead-of-print 21 December 2016

Aims (i) to evaluate a novel hybrid near-infrared fluorescence—intravascular ultrasound (NIRF-IVUS) system in coronary and peripheral swine arteries *in vivo*; (ii) to assess simultaneous quantitative biological and morphological aspects of arterial disease.

Methods and results Two 9F/15MHz peripheral and 4.5F/40MHz coronary near-infrared fluorescence (NIRF)-IVUS catheters were engineered to enable accurate co-registrtation of biological and morphological readings simultaneously *in vivo*. A correction algorithm utilizing IVUS information was developed to account for the distance-related fluorescence attenuation due to through-blood imaging. Corrected NIRF (cNIRF)-IVUS was applied for *in vivo* imaging of angioplasty-induced vascular injury in swine peripheral arteries and experimental fibrin deposition on coronary artery stents, and of atheroma in a rabbit aorta, revealing feasibility to intravascularly assay plaque structure and inflammation. The addition of ICG-enhanced NIRF assessment improved the detection of angioplasty-induced endothelial damage compared to standalone IVUS. In addition, NIRF detection of coronary stent fibrin by *in vivo* cNIRF-IVUS imaging illuminated stent pathobiology that was concealed on standalone IVUS. Fluorescence reflectance imaging and microscopy of resected tissues corroborated the *in vivo* findings.

Conclusions Integrated cNIRF-IVUS enables simultaneous co-registered through-blood imaging of disease related morphological and biological alterations in coronary and peripheral arteries *in vivo*. Clinical translation of cNIRF-IVUS may significantly enhance knowledge of arterial pathobiology, leading to improvements in clinical diagnosis and prognosis, and helps to guide the development of new therapeutic approaches for arterial diseases.

Keywords IVUS • NIRF • molecular imaging • fluorescence imaging

Introduction

Intravascular ultrasound (IVUS) and intravascular optical coherence tomography (IVOCT) are widely utilized clinical imaging modalities employed for the diagnosis and treatment of coronary artery and peripheral vascular disease. First clinically tested in 1989,[1] IVUS is currently the most often utilized intravascular imaging tool, capable of acquiring data through the entire vessel wall in the presence of blood, although at a relatively slow pull back rate of 0.5–1.0 mm/sec.[2] IVOCT, on the other hand, offers superb pullback speeds up to

* Corresponding author. Tel: 6177249353; Fax: 16178603180. E-mail: fjaffer@mgh.harvard.edu

† Bozhko and Osborn share first authorship

‡ Jaffer and Ntziachristos share senior authorship

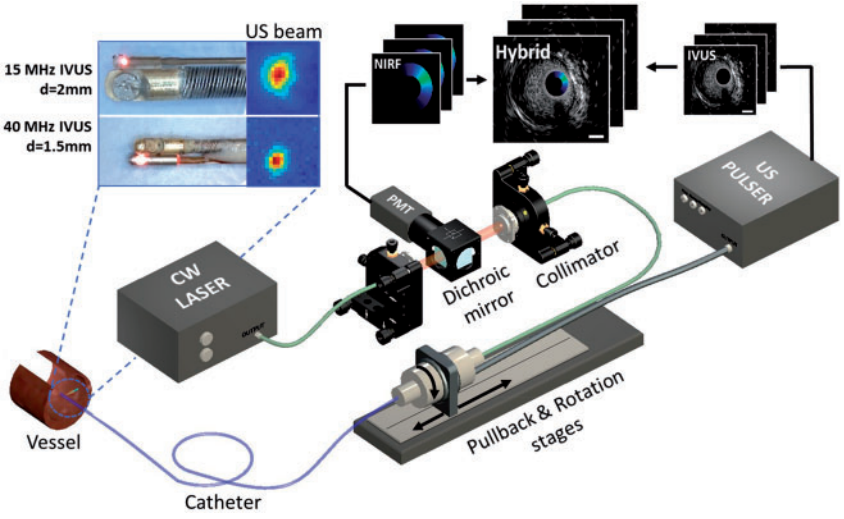

Figure 1 Schematic of the cNIRF-IVUS imaging system for intravascular through-blood imaging. The cNIRF-IVUS imaging catheters (insets on top left) consist of a 9F/15MHz ultrasound transducer and NIRF optical fiber for imaging larger peripheral arteries, or a 4.5F/40MHz transducer with optical fiber for imaging smaller coronary arteries. The dual-modality imaging probe rotates and pulls back inside a transparent catheter sheath through the use of an electro-optical rotary joint, which connects the moving catheter with the stationary back-end console. The hybrid image is reconstructed by combining structural ultrasound information with precisely co-registered NIR fluorescence emission signals.

40 mm/sec and excellent imaging resolution, but has limited penetration depth and requires lumen flushing to displace blood from the imaging field.[3,4] Although both IVUS and IVOCT can interrogate structural features of atherosclerotic plaques and stents,[4] neither modality routinely reveals the pathobiological features that drive arterial disease onset, progression, and complication.[5,6]

Enrichment of IVUS and IVOCT data with cellular and molecular information holds great potential towards improved understanding of the biology and mechanisms of vascular disease in living subjects and the assessment of novel anti-atherosclerosis pharmaceuticals and endovascular therapies.[7–11] Near-infrared fluorescence (NIRF) imaging is emerging as a highly promising approach with major translational applications for diagnosis and management of cardiovascular disease, due to its capacity to detect molecular reporters *in vivo* at high sensitivity within human coronary-sized arteries.[12–14] However, two main features limit standalone applications of intravascular NIRF imaging: (i) it does not provide detailed structural information and (ii) uncorrected NIRF images do not accurately quantify the concentration of fluorophores, due to the variable amount of blood attenuation of the NIRF signal between the vessel wall and the catheter. Therefore, for accurate quantitative applications, NIRF measurements must be paired with a precisely co-registered structural imaging modality and an algorithm that can correct for the distance-dependent light attenuation in blood.[15] The combination of NIRF and IVUS in a single intravascular catheter system has been previously implemented,[16] but did not demonstrate feasibility of intracoronary imaging, and further relied on static *ex vivo* or empirical blood attenuation parameters that do not accurately represent NIR light attenuation in flowing blood *in vivo*, and possibly varying hematocrit. This early report has not explored the technical possibility of employing integrated NIRF-IVUS imaging in coronary arteries and stents *in vivo*, which are key determinants for research use and clinical translation of NIRF-IVUS imaging. Importantly earlier work has not addressed the quantification accuracy of NIRF-IVUS in regard to adaptive attenuation readings accounting for the effective blood attenuation *in vivo*.

In this study, we developed a cNIRF-IVUS (c = corrected) integrated imaging approach to accurately account for NIRF light attenuation in flowing blood in swine peripheral and coronary arteries *in vivo*. We hypothesized that IVUS-guided NIRF image reconstruction with a measurement-driven adaptive attenuation algorithm would yield rigorous quantitative readings of NIR fluorescence from the vessel wall. We experimentally interrogated the merits of the hybrid cNIRF-IVUS modality with phantom measurements. Then, we evaluated the ability of cNIRF-IVUS to detect *in vivo* pathobiology of vascular injury, clinical-grade stents in swine peripheral and coronary arteries and atheroma-associated inflammation.

Methods

Construction and validation of the cNIRF-IVUS system for biological and morphological intravascular imaging *in vitro*

The cNIRF-IVUS intravascular imaging system was established in our laboratory for simultaneous NIR fluorescence and ultrasound through-blood measurements *in vivo*, using 4.5 French (1.5 mm diameter) coronary artery and 9 French (3 mm diameter) peripheral artery catheters (*Figure 1*). The experimental setup consisted of two major components: (i) the back-end console, which drives the ultrasound and optical elements and collects the data and (ii) the front-end intravascular catheters. The back-end console of the cNIRF-IVUS system utilized a continuous wave (CW) laser source with a central wavelength of 750 nm and an

ultrasound pulser-receiver unit with a built-in amplifier. In order to interface the optical and electrical signals from the back-end console to the catheter system, a rotary joint was designed and custom built. The latter offers (i) direct fiber-to-fiber light coupling through precise alignment between the stationary and rotating fibers; (ii) transmission and reception of the ultrasound readouts by coupling electrical signals through a concentric slip ring built around the fiber. To achieve high sensitivity fluorescence detection enabling through-blood NIRF imaging, we employed a 6-stage amplification extended multi-alkali photomultiplier tube (PMT) adapted with a set of NIR fluorescence filters. As the size, penetration depth, and resolution of IVUS modality depends on the central excitation frequency, two front-end intravascular cNIRF-IVUS catheters were designed: one for the larger peripheral arteries (diameter $>$ 5 mm), and another for the coronary arteries (diameter $<$ 5 mm). The larger-sized cNIRF-IVUS catheter utilized a 15 MHz transducer integrated with the optical fiber, resulting in a full outer diameter of 3.0 mm (9 French). The coronary-sized cNIRF-IVUS catheter employed a 40 MHz transducer integrated with the optical fiber, resulting in an outer diameter of 1.5 mm (4.5 French). During helical (rotational plus translational) pullback scanning, the hybrid cNIRF-IVUS catheters sampled structural depth profiles (A-lines) and corresponding NIR fluorescence intensities. Rotation (80, 120 or 160 turns per min) and translation were automatically driven by mechanical stages at a pitch scanning helix (pullback step size along the vessel) of 0.2 mm, resulting in pullback speeds of 0.3, 0.4, or 0.53 mm/sec. Ultrasound and optical beams were aligned (relative angle $<$ 7 degrees) so that catheter acquired precisely co-registered IVUS and NIRF signals from the same area. The characterization of cNIRF-IVUS system is presented in Supplementary data online, *S1*.

Fluorescence intensity correction for blood attenuation *in vivo*

A correction algorithm was developed to adjust the NIRF readouts for distance-dependent light attenuation in blood. The algorithm was based on the Twersky model for transmission measurements[17] (Supplementary data online, *Information S2*). We discovered that distance-correction model calibrated empirically on *ex vivo* data overestimates the degree of light attenuation that occurs *in vivo* (Supplementary data online, *Figure S2*). Therefore, we based our distance-correction calibration solely on *in vivo* attenuation measurements and demonstrated that cNIRF-IVUS is capable of detecting changes of blood absorption due to hematocrit variations, enabling adaptive correction on a per measurement basis (Supplementary data online, *Information S3*).

Intravascular cNIRF-IVUS *in vivo* imaging of arterial disease

Male Yorkshire pigs (13–15 weeks old, 40–47 kg, $N = 8$, MGH IACUC Protocol # 2012N000066) were used for pilot cNIRF-IVUS imaging studies. Animals were anesthetized with telazol (4.4 mg/kg) and xylazine (2.2 mg/kg), followed by isoflurane (Patterson Veterinary Supply, Devens, MA, USA). The electrocardiogram (ECG), oxygen saturation and invasive arterial blood pressure were monitored throughout the experimental procedure.

a) Validation of cNIRF-IVUS *in vivo* detection of model NIR fluorophores

In the first study, the repeatability of cNIRF-IVUS imaging was examined using through-blood *in vivo* imaging of an NIR fluorophore deposited directly inside the artery wall ($N = 2$). After surgical exposure, a 6F introducer sheath was placed into the distal carotid artery. A NIR fluorophore (AlexaFluor 750, 0.2 mL, concentration 50 μM) was injected directly into the outer wall of the proximal carotid artery to simulate targeted fluorophore accumulation. The 4.5F/40MHz cNIRF-IVUS catheter was then inserted through the sheath into the proximal carotid artery, and three sequential cNIRF-IVUS pullbacks were performed. Between each pullback, the catheter was re-advanced to the same starting position using X-ray fluoroscopic guidance. The combined cNIRF-IVUS data set was presented as a video file (Supplementary data online, *Video 1*) and a co-registered 3D-rendered image of the lumen and fluorescence activity (*Figure 2D*). After *in vivo* experiments the vessel underwent *ex vivo* fluorescence reflectance imaging (FRI) for validation purpose. Here and in other experiments, *in vivo* and *ex vivo* images were co-registered and therefore (i) scaled to represent the same region of interest; (ii) aligned using either rigid transformation function in ImageJ or manually, based on visual affinity.

b) *In vivo* cNIRF-IVUS imaging of peripheral arterial injury induced by angioplasty

In the second study, angioplasty-induced vascular injury was imaged *in vivo* in mechanically injured swine peripheral arteries ($N = 3$). The distal femoral arteries (average diameter 3.1 mm based on in vivo IVUS measurements) of two animals were interrogated with the 4.5F/40MHz catheter (presented in Supplementary data online, *Information S5*). To explore the performance of the bigger peripheral catheter that was designed with an enhanced penetration depth to visualize the entire vessel wall, the larger proximal iliac artery (average diameter 6.8 mm based on in vivo IVUS measurements) of one animal was imaged with the 9F/15MHz cNIRF-IVUS. In the latter case, intra-arterial access was achieved with a 9F introducer sheath in the right femoral artery. A 4.0×20 mm angioplasty balloon was inflated to 10 atm three times in the right iliac artery for one minute per inflation. Subsequently, indocyanine green (ICG, 0.25 mg/kg, i.v.) was administered to assess for impaired endothelial permeability following angioplasty. Ninety minutes later, a cNIRF-IVUS pullback over 40 mm vessel length was performed at pullback speed 0.5 mm/sec, starting proximal to the injury site and ending in the distal portion of the right iliac artery outside the injured segment.

c) *In vivo* intracoronary cNIRF-IVUS imaging of fibrin deposition on coronary artery stents

In the third study, a 2.75 × 12 mm coronary bare metal stent bearing NIR fluorescent-fibrin was implanted into the right coronary artery of swine and imaged using the 4.5F/40MHz cNIRF-IVUS catheter ($N = 3$). To prepare the NIRF stent, human clots were created from fresh frozen plasma (FFP) obtained via a protocol approved by the Partners Institutional Review Board (#2004P001401). A centrifuge tube was filled with 180 μL of FFP. The stent was next immersed into the FFP and then 10 μL of 0.4 M $CaCl_2$, 10 μL of thrombin, and 12 μL of FTP11-Cy7 were added with brief mixing followed by incubation at 37 °C for approximately 24 h to induce clot formation around the stent.[18] After coronary implantation of the NIR fluorescent fibrin-coated stent, a 30 mm long cNIRF-IVUS imaging pullback was performed with a rotational speed 80 rpm (pullback speed 0.3 mm/sec). Such a rotation speed was chosen in order to match the heart rate and thus potentially reduce motion artifacts.[19,20] Additional histology and fluorescence microscopy of resected swine coronary artery with NIRF fibrin-coated stents was performed (Supplementary data online, *Information S6*).

d) *In vivo* intravascular cNIRF-IVUS imaging of atheroma inflammation

In addition, we demonstrated the ability of the 40MHz cNIRF-IVUS system to identify inflammatory protease activity in rabbit aortic atheroma (Supplementary data online, *Information S7*).

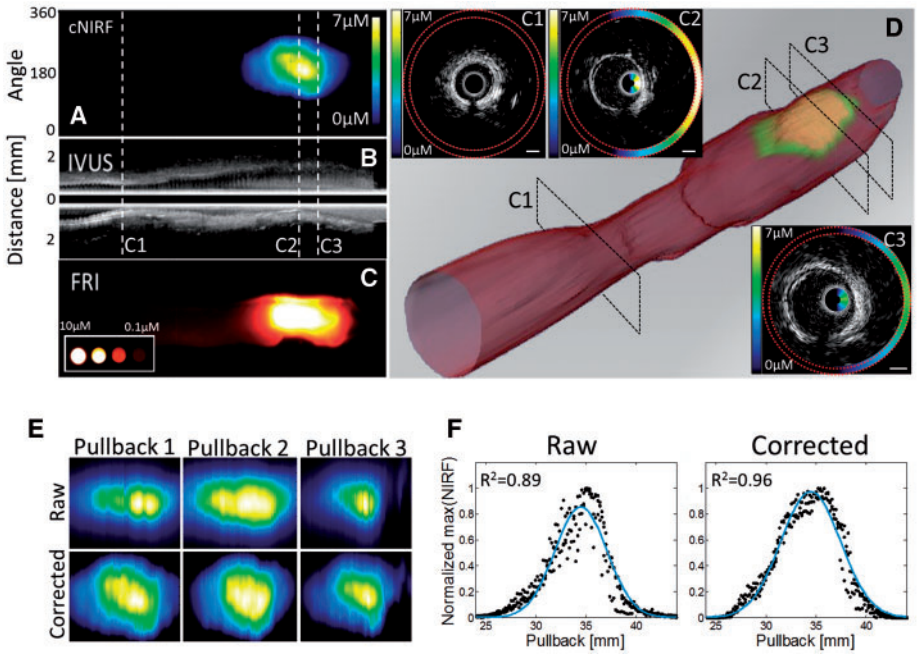

Figure 2 Intravascular cNIRF-IVUS imaging with the 4.5F/40MHz catheter reveals the value of IVUS-based distance correction of the NIRF signal in blood. *In vivo* cNIRF-IVUS imaging of a swine carotid artery was performed following local injection of an NIR fluorophore into the artery wall. Panels (*A*), (*B*) and (*C*) illustrate the *in vivo* cNIRF image, the corresponding longitudinal IVUS image, and the FRI image of the resected artery, respectively. (*D*) A 3D representation of the lumen and arterial wall NIR fluorescence signal rendered based on the *in vivo* cNIRF-IVUS image stack. Insets (C1–C3) show representative examples of the cross-sectional cNIRF-IVUS images corresponding to pullback positions C1, C2, and C3 in (B), (C), and (D). The cNIRF signal in C1, C2, and C3 is fused onto the interior of the IVUS catheter and also replicated at the exterior (outlined with red dotted lines) of the IVUS image. (*E*) Serial imaging of the same vessel region demonstrates that the raw NIRF signal (top row) is affected by variable intraluminal catheter position that changes the distance between the NIR fluorescence source and imaging catheter detector, leading to fluctuations in the measured NIRF signal. Note that applying the NIRF distance correction (bottom row) substantially improved the reproducibility of the NIRF image and reduced the variability due to changes in catheter position. (*F*) Quantitative assessment of the improvement of the reproducibility by NIRF distance correction: black dots correspond to the maximum NIRF signal vs. pullback position, and the blue line indicates the average distribution function. Distance correction improved the correspondence between NIRF signals from all three pullbacks from $R^2 = 0.89$ to $R^2 = 0.96$.

Results

In vitro assessment of cNIRF-IVUS catheter performance and distance correction

The NIRF catheter angular resolution at 1 mm through blood was 24° (15 sectors); the ultrasound axial and lateral resolution was 270 μm and 500 μm, respectively, for the 9F/15MHz catheter, and 150 μm and 240 μm, respectively, for the 4.5F/40MHz catheter (Supplementary data online, *Figure S1*). The NIRF catheter could detect 200 nM of NIR fluorophore (AlexaFluor 750) at distances < 2 mm. Correction for blood attenuation of the NIRF signal was derived from *in vivo* blood measurements and generated a lookup table for distance correction of the NIRF signal (Supplementary data online, *Figures S2 and S3*) used in subsequent *in vivo* experiments.

Concurrent NIRF and IVUS imaging of the intravascular arterial environment

First, we demonstrated the feasibility and reproducibility of through-blood cNIRF-IVUS *in vivo* imaging (*Figure 2*). *Figure 2A and 2B* show co-registered fluorescence and ultrasound images, respectively, of a carotid artery with a NIR fluorophore injected into the artery wall. *Figure 2C* displays a post-mortem fluorescence reflectance image (FRI) of the same artery resected from the animal (with blood flushed) after completion of the *in vivo* imaging procedure, for validation purposes. Second, we assessed the reproducibility of through-blood NIRF imaging data acquisition. The NIRF images from three pullbacks before and after distance correction are shown in *Figure 2E*. Although the same region of the vessel was scanned, visible discrepancies are evident amongst the uncorrected NIRF images (*Figure 2E*, top row). This finding can be explained by the varying intraluminal catheter position after catheter re-advancements and movements due to blood fluxes and respiratory motion. Additionally, the effect of the heartbeat (cardiac motion) on the NIRF signal appears as interleaved vertical lines (*Figure 2E*). We measured the attenuation of the NIR fluorescence signal arising from the cardiac cycle to be up to −4.5dB. To see whether distance correction could substantially improve the consistency of the NIRF results, we implemented a correction algorithm to every catheter pullback (*Figure 2E*, bottom row). The correcting effect was quantitatively assessed by computing the

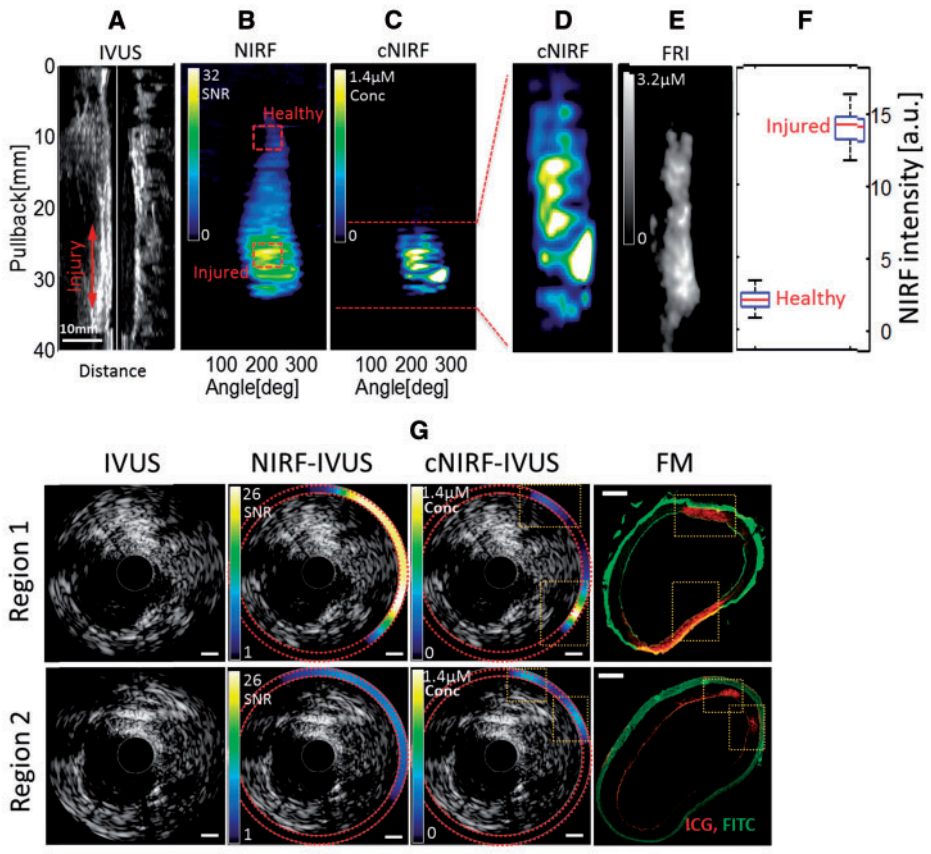

Figure 3 *In vivo* cNIRF-IVUS imaging of vascular injury with ICG in a swine iliac artery using the 9F/15MHz hybrid cNIRF-IVUS catheter. (*A*) Ultrasound longitudinal image of the injured artery; (*B, C*) the corresponding raw NIRF image of ICG-demarcated vascular injury induced by the angioplasty balloon before and after correction. Note, that unlike IVUS, NIRF shows clear demarcation of injured region labelled by ICG. (*D*) Expanded view of the distance-corrected NIRF signal from the injured area of the artery. (*E*) FRI of the resected injured iliac artery corresponded well with the *in vivo* distance-corrected cNIRF image shown in panel (D). (*F*) NIRF signal specificity was assessed by comparing NIRF intensities from healthy and injured areas of the vessel marked with red dashed squares in panel (B). On each box, the central red mark is the median value, the edges of the box are the 25th and 75th %, and the whiskers extend to the most extreme data points. (*G*) Comparison of the standalone IVUS, and the integrated cNIRF-IVUS cross sectional images before and after blood attenuation correction with FM micrographs of anatomically matched tissue sections. Note that injury is not apparent by structural imaging with standalone IVUS. In comparison, injury demarcated by ICG deposition is clearly recognized on the cNIRF-IVUS merged images in Region 1 and Region 2, as confirmed by FM (orange dotted boxes; red pseudocolor = ICG, green pseudocolor = FITC autofluorescence). Scale bars in NIRF and cNIRF images, 1 mm. Scale bar in FM images, 0.5 mm.

cross-correlation of the NIRF signals from all scans (*Figure 2F*). As shown, distance correction improved the correspondence between NIRF signals from all three pullbacks from $R^2 = 0.89$ to $R^2 = 0.96$. The effect of the heartbeat (cardiac motion) on the NIR fluorescence signal decreased to −1.4 dB. To further demonstrate specificity of the cNIRF modality to fluorescence activity, we also imaged background NIRF signal in an uninjured (healthy) vessel (Supplementary data on line, *Information S4*), where ~35 times less NIRF signal was detected, compared to the area injected with a NIR fluorophore.

cNIRF-IVUS detection of angioplasty-induced arterial injury

Percutaneous transluminal angioplasty, a mainstay treatment of clinically obstructive atherosclerosis, can induce vascular injury that may not be readily visualized with conventional imaging methods such as standalone IVUS. We investigated whether cNIRF-IVUS could detect angioplasty-induced vascular injury in peripheral swine arteries *in vivo*, beyond that detectable by IVUS alone. After balloon injury of a swine peripheral artery (see Methods), ultrasound images obtained *in vivo* (*Figure 3A*) did not indicate any evidence of arterial injury. However, simultaneously acquired NIRF images (*Figure 3B*) following administration of indocyanine green (ICG) demonstrated ICG NIRF signal accumulation in the areas of the angioplasty-induced vascular injury, indicating zones of impaired endothelial barrier integrity secondary to local damage of the arterial wall, similar to atheroma with impaired endothelial barrier function.[21] The target-to-background ratio between fluorescence intensities collected from the injured and healthy vessel areas (highlighted with red dashed squares in *Figure 3B*) was 24 dB (*Figure 3F*). Distance-corrected cNIRF images (*Figure 3C and D*)

revealed more focal NIR fluorescence ICG signal deposition, which visually corresponded better with the NIR fluorescence readouts obtained with FRI imaging of the excised arterial specimen (*Figure. 3E*). It should be noted however, that quantitative comparison between cNIRF and FRI images is limited, since cNIRF captures fluorescence from within the vessel lumen, while FRI is surface-weighted to fluorescence outside of the vessel. To quantify the effect of distance correction, we compared axial cNIRF-IVUS images with corresponding fluorescence microscopy (FM) tissue section slides. As shown in *Figure 3G*, distance correction improved the correspondence between *in vivo* cNIRF signals and ICG NIRF fluorescence (red) obtained with FM from $R = 0.36$ to $R = 0.58$ in Region 1 and from $R = 0.61$ to $R = 0.69$ in Region 2.

cNIRF-IVUS Biological Imaging of Fibrin Deposition on Implanted Coronary Stents

To further demonstrate potential of the cNIRF-IVUS system for imaging pathobiological features of coronary-sized arteries, we evaluated whether cNIRF-IVUS could detect *in vivo* NIRF signals from a fibrin-targeted probe (FTP11) on coronary artery stents implanted in swine. While standalone IVUS revealed the architecture of the coronary artery and stent (*Figure 4A*), IVUS could not specifically identify stent fibrin deposition. In contrast, co-registered cNIRF images acquired simultaneously with IVUS allowed *in vivo* visualization of stent NIRF fibrin deposition (*Figure 4B and 4C*). In this experiment, the rotation speed of the catheter was chose to be close to the intrinsic heart rate. However, as it was not synchronized with the cardiac cycle, catheter motions arising from the heartbeat were still present. *Figure 4H* shows representative cNIRF-IVUS cross sections in pullback positions S1, S2 and S3. When compared to FRI of excised stent tissue (*Figure 4D*), good visual correlation of the NIR fluorescence distribution was observed within the stented region. Fluorescence microscopy of the resected stent lumen surface after opening the stent longitudinally (*Figure 4G*) showed similar NIRF fibrin deposition patterns to *in vivo* NIRF (*Figure 4E*) and cNIRF images (*Figure 4F*). Application of NIRF distance correction quantitatively improved the correlation coefficient between FM and *in vivo* NIRF images from $R = 0.68$ (NIRF) to $R = 0.74$ (cNIRF). In addition, the cNIRF distance correction algorithm recovered some fine details of the fluorescence image (*Figure. 4F*, areas 1 and 2) that were not visible on the raw NIRF images (*Figure 4E*, areas 1 and 2).

Discussion

IVUS and IVOCT are the current mainstay intra-arterial clinical imaging modalities that assay morphological features, but do not routinely assess biological information underlying vascular diseases. The engineering and *in vivo* validation of cNIRF-IVUS enriches IVUS data with pathobiological detail that may convey important clinical and translational information. The results here provide new evidence that intracoronary and intra-large artery data that simultaneous integrated NIRF-US biological-structural imaging can be performed *in vivo*. To improve the accuracy of NIRF imaging, we employed an *in vivo* data-driven NIRF correction to account for a NIRF signal discrepancy related to the position of the catheter within the vessel. Compared to standalone IVUS, cNIRF-IVUS readily identified areas of ICG uptake in areas of angioplasty-induced injury, FTP11-positive fibrin deposition on coronary artery stents, and inflammatory protease activity in atherosclerosis *in vivo*. Detection of *in vivo* vascular pathobiology by cNIRF-IVUS beyond standalone IVUS offers a novel and powerful imaging approach for research of vascular injuries, and extends the applications of ICG and related targeted NIRF imaging probes beyond atherosclerosis detection.[22] Intravascular detection of stent fibrin deposition with cNIRF FTP11 imaging may lead to early recognition and diagnosis of unhealed stent struts at risk for stent thrombosis.[23,24]

While IVUS remains the predominant clinical intracoronary imaging approach, the potential significance of hybrid intravascular approaches [25] has been underscored by recent developments such as multimodal NIRF-IVOCT systems [14] and NIR spectroscopy (NIRS)-IVUS systems.[26] A comparison of NIRF-IVUS and NIRF-OCT is warranted, as both methods are options for intravascular molecular imaging.[10] Intravascular NIRF-OCT is a validated multimodal approach [27] that offers integrated anatomical-molecular imaging with superior resolution and speed (tens of micrometers, 20–40 mm/sec pullback speed) compared to IVUS (hundreds of micrometers, 0.5–1.0mm/sec pullback speed). However, the OCT component of NIRF-OCT requires flushing to displace blood from the imaging field, typically with iodinated contrast, which limits OCT's applicability to patients with impaired renal function. In addition, the lower depth of penetration of OCT also precludes some applications such as plaque burden quantification and imaging of larger-sized arteries such as the left main. Finally, as IVUS is still the predominant clinical intravascular imaging modality, the availability of both complementary NIRF-IVUS and NIRF-OCT systems will help accelerate the development of clinical intravascular NIRF applications. In comparison to other hybrid optical imaging modalities such as optoacoustics [28] or spectral imaging,[29] or NIRS-IVUS, cNIRF-IVUS offers improved flexibility and specificity due to the increasing availability of exogenous NIR fluorescent agents with specificity to a wide range of important biological processes, such as altered vascular permeability and endothelial inflammation,[22] tissue protease activity,[12] apoptotic markers and other biomarkers of vascular pathologies.[8,30] In addition to FDA-approved NIRF agents such as ICG, new targeted NIRF reporters are now being safely tested in animal models and patients.[31]

Compared to a prior single *in vivo* NIRF-IVUS study performed in rabbit aortas,[16] the current study demonstrates the ability to perform integrated NIRF-IVUS in the coronary and peripheral arteries, the main targets of clinical intravascular imaging approaches. In addition, the prior study relied on correction of blood attenuation by parameters derived from *ex vivo* observations or empirical measurements. In contrast the present analysis utilized *in vivo* session-specific estimation of blood attenuation (Supplementary data online, *Information S3–S4*), and found that blood attenuation was not as severe compared to *ex vivo* approximations, and markedly changed the quantitative results of the NIRF portion of the study. This new approach makes cNIRF-IVUS more accurate and adaptable to specific measurements in the *in vivo* environment. Additionally, we quantified the attenuation of the NIRF intensity arising from heartbeat (cardiac) motion to be up to -4.5 dB in carotid arteries. This effect was reduced by factor of ~ 3 (to -1.4 dB) after applying the distance correction algorithm. Furthermore, there is an unmet need to identify biological

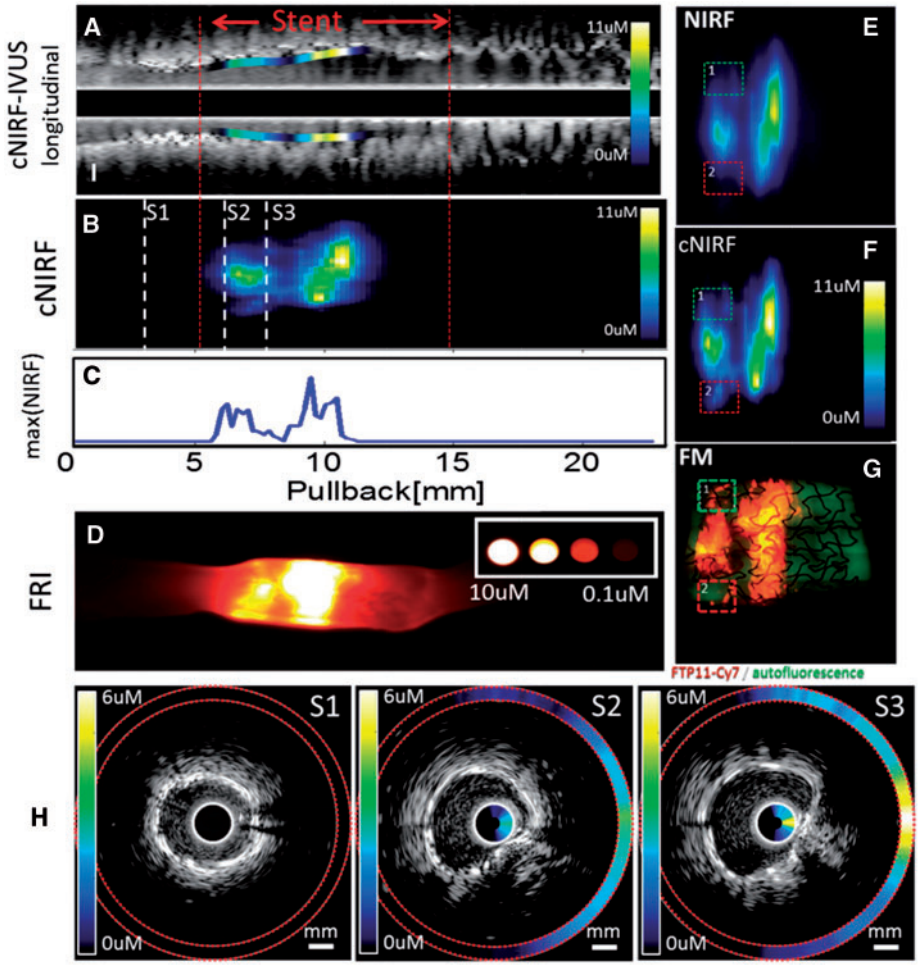

Figure 4 *In vivo* imaging of the coronary artery with an implanted NIR fluorescent fibrin-labelled stent using the 4.5F/40MHz hybrid cNIRF-IVUS catheter. (*A*) Longitudinal cNIRF-IVUS fusion image of the artery. (*B*) Distance-corrected cNIRF signal measured *in vivo* through blood from the same artery shown in panel (a). (*C*) Intensity profile of NIRF concentration as function of NIRF catheter pullback position. (*D*) FRI of the resected coronary artery shown in panels (a) and (b). (*E, F*) Expanded view of the uncorrected and corrected NIRF image across the stented region, with (*G*) corresponding FM of the resected stent lumen surface after opening the stent longitudinally (red/orange pseudocolor = FTP11-Cy7 NIRF fibrin signal; green pseudocolor = FITC autofluorescence). Note that area 1 and 2 in (G) were not visible on the raw NIRF image (E), but were recovered as result of distance correction (F). Quantitative image analysis demonstrated good correlation between *in vivo* cNIRF (F) and resected stent FM (G) images ($R = 0.74$), that were improved compared to the raw NIRF and FM images ($R = 0.68$). (*H*) Representative cross-sectional cNIRF-IVUS images corresponding to pull back positions S1, S2, and S3 from panel (B). The cNIRF signal is fused on to the interior of the IVUS catheter and also the exterior boundary of the IVUS image (highlighted by red dotted lines). Scale bars, 1 mm.

mechanisms of action in coronary artery disease to help gauge the potential success of new pharmacotherapeutics for CAD. While standalone IVUS has been used to assess changes in plaque burden as a surrogate marker for drug efficacy in CAD, [32] there are currently minimal options to assess changes in coronary arterial plaque biology in response to CAD drug therapy. The developed cNIRF-IVUS strategy enables integrated molecular and structural assessment of new CAD treatments and is well positioned to help assess the biological efficacy of new drugs in phase II and III clinical trials.

Study limitations. Due to the study focus on engineering a new imaging system and establishing proof-of concept for translational imaging *in vivo*, the experimental sample size was limited to cNIRF-IVUS imaging of the carotid, coronary, and peripheral arteries of $n = 8$ swine. Additionally, cNIRF-IVUS was successfully performed in rabbits with inflammatory atherosclerosis, with a representative example shown in Supplementary data online, *Information S7*. Further dedicated preclinical studies with larger numbers of animals are planned to understand the *in vivo* biology of atherosclerosis progression and stent complications in medium and larger sized arteries. Second, while the diameter of the current prototype 4.5F/40MHz cNIRF-IVUS is of larger diameter than clinical IVUS systems (3–3.5F), strategies to miniaturize catheter components and to better integrate the optical and ultrasound front-end are anticipated to reduce the cNIRF-IVUS diameter to 3F (1.0mm). Third, due to limitations of

scaling customized NIRF agent doses for intravenous use in large-sized swine, the coronary stents utilized for *in vivo* swine coronary artery cNIRF-IVUS imaging were directly labelled with the FTP11 NIRF fibrin agent *ex vivo* before implantation. Fourth, the correction algorithm implemented in this study depends on accurate measurement of distances by IVUS and thus is prone to errors related to IVUS image acquisition, including motion artefacts and low signal to noise ratio; however, this limitation could be surpassed with development of faster and more effective ultrasound detectors in the next generation cNIRF-IVUS system. Finally, the current NIRF sensitivity enable the maximum NIRF imaging distance to ~2 mm through blood. This imposes an upper limit on vessel diameter 4–5 mm (depending on the diameter of the NIRF-IVUS catheter itself) that can be reliably imaged with a centred 4.5F/40MHz catheter. Of note, however, this diameter is likely suitable for the majority of coronary arteries that undergo IVUS imaging; furthermore, in the presence of arterial stenosis with plaques, the luminal diameter will be lower, further increasing the potential for reliable NIRF signal detection. In the future, the sensitivity of fluorescence detection can be enhanced by system re-engineering incorporating optical fibers with a bigger core diameter and/or numerical aperture. Such engineering modifications should serve to increase SNR and therefore, the achievable imaging depth through blood.

The results presented herein demonstrate the feasibility of concurrent cNIRF-IVUS imaging in swine coronary and peripheral artery and rabbit aorta, enabling quantitative detection of vascular biology and structural detail through blood *in vivo*. The addition of NIRF biological imaging capabilities to IVUS offers new insights into arterial injury, atheroma inflammation, and stent pathology *in vivo* in a single catheter pullback identical to IVUS workflows. With the anticipated clinical translation of this new technology, cNIRF-IVUS has the potential to aid in the detection of high-risk plaques and high-risk stents, and help facilitate pharmacotherapeutic trials for atherosclerosis.

Conflicts of interest: Jaffer has received research funding from Siemens, Merck and Kowa, and has a consulting agreement with Boston Scientific and Abbott Vascular. Massachusetts General Hospital has a patent licensing arrangement with Canon Corporation. Jaffer has the right to receive licensing royalties through this licensing arrangement. DB, EAO, AR, JWV, TH, SK, GW, SVO, JRM, AM, AFS, and VN have no conflicts to declare.

Funding

This work was supported by the Deutsche Forschungsgemeinschaft (DFG; RO 4268/4-1) and by the European Union project PRESTIGE (FP7, #260309), National Institutes of Health (NIH) R01 HL108229 and R01 HL122388-01A1 (F.A.J.), American Heart Association (#13POST14640021 to T.H.; #12PRE11160000 to A.F.S, #13GRNT17060040 to F.A.J), MGH Hassenfeld Research Scholar Fund, Rubicon Grant 825.12.013/ Netherlands Organization for Scientific Research (JWV), the Kanae Foundation for Research Abroad (TH), and the Harvard Catalyst NIH 1UL1 TR001102-01 (EAO).

References

1. Hodgson JM, Graham SP, Savakus AD, Dame SG, Stephens DN, Dhillon PS *et al.* Clinical percutaneous imaging of coronary anatomy using an over-the-wire ultrasound catheter system. *Int J Card Imaging* 1989;**4**:187–93.
2. Garcia-Garcia HM, Costa MA, Serruys PW. Imaging of coronary atherosclerosis: intravascular ultrasound. *Eur Heart J* 2010;**31**:2456–69.
3. Yabushita H, Bouma BE, Houser SL, Aretz HT, Jang IK, Schlendorf KH *et al.* Characterization of human atherosclerosis by optical coherence tomography. *Circulation* 2002;**106**:1640–5.
4. Tearney GJ, Regar E, Akasaka T, Adriaenssens T, Barlis P, Bezerra HG *et al.* Consensus standards for acquisition, measurement, and reporting of intravascular optical coherence tomography studies: a report from the international working group for intravascular optical coherence tomography standardization and validation. *J Am Coll Cardiol* 2012;**59**:1058–72.
5. Libby P, Ridker PM, Hansson GK. Progress and challenges in translating the biology of atherosclerosis. *Nature* 2011;**473**:317–25.
6. Tabas I, Glass CK. Anti-inflammatory therapy in chronic disease: challenges and opportunities. *Science* 2013;**339**:166–72.
7. Jaffer FA, Libby P, Weissleder R. Molecular imaging of cardiovascular disease. *Circulation* 2007;**116**:1052–61.
8. Sanz J, Fayad ZA. Imaging of atherosclerotic cardiovascular disease. *Nature* 2008;**451**:953–7.
9. Osborn EA, Jaffer FA. The advancing clinical impact of molecular imaging in CVD. *JACC Cardiovasc Imaging* 2013;**6**:1327–41.
10. Mulder WJM, Jaffer FA, Fayad ZA, Nahrendorf M. Imaging and nanomedicine in inflammatory atherosclerosis. *Sci Transl Med* 2014;**6**:239sr1.
11. Chen IY, Wu JC. Cardiovascular molecular imaging: focus on clinical translation. *Circulation* 2011;**123**:425–43.
12. Jaffer FA, Calfon MA, Rosenthal A, Mallas G, Razansky RN, Mauskapf A *et al.* Two-dimensional intravascular near-infrared fluorescence molecular imaging of inflammation in atherosclerosis and stent-induced vascular injury. *J Am Coll Cardiol* 2011;**57**:2516–26.
13. Vinegoni C, Botnaru I, Aikawa E, Calfon MA, Iwamoto Y, Folco EJ *et al.* Indocyanine green enables near-infrared fluorescence imaging of lipid-rich, inflamed atherosclerotic plaques. *Sci Transl Med* 2011;**3**:84ra45.
14. Yoo H, Kim JW, Shishkov M, Namati E, Morse T, Shubochkin R *et al.* Intra-arterial catheter for simultaneous microstructural and molecular imaging *in vivo*. *Nat Med* 2011;**17**:1680–4.
15. Mallas G, Brooks DH, Rosenthal A, Nudelman RN, Mauskapf A, Jaffer FA *et al.* Improving quantification of intravascular fluorescence imaging using structural information. *Phys Med Biol* 2012;**57**:6395–406.
16. Abran M, Stähli BE, Merlet N, Mihalache-Avram T, Mecteau M, Rhéaume E *et al.* Validating a bimodal intravascular ultrasound (IVUS) and near-infrared fluorescence (NIRF) catheter for atherosclerotic plaque detection in rabbits. *Biomed Opt Express* 2015;**6**:3989.
17. Twersky V. Absorption and multiple scattering by biological suspensions. *J Opt Soc Am* 1970;**60**:1084–93.
18. Hara T, Bhayana B, Thompson B, Kessinger CW, Khatri A, McCarthy JR *et al.* Molecular imaging of fibrin deposition in deep vein thrombosis using fibrin-targeted near-infrared fluorescence. *JACC Cardiovasc Imaging* 2012;**5**:607–15.
19. Bruining N, Von Birgelen C, De Feyter PJ, Ligthart J, Li W, Serruys PW *et al.* ECG-gated versus nongated three-dimensional intracoronary ultrasound analysis: implications for volumetric measurements. *Cathet Cardiovasc Diagn* 1998;**43**:254–61.
20. von Birgelen C, de Vrey EA, Mintz GS, Nicosia A, Bruining N, Li W *et al.* ECG-gated three-dimensional intravascular ultrasound: feasibility and reproducibility of the automated analysis of coronary lumen and atherosclerotic plaque dimensions in humans. *Circulation* 1997;**96**:2944–52.
21. Verjans JW, Osborn EA, Ughi GJ, Calfon Press MA, Hamidi E, Antoniadis AP *et al.* Clinical and intracoronary evaluation of indocyanine green for targeted near-infrared fluorescence imaging of atherosclerosis. *JACC Cardiovasc Imaging* 2016;**9**:1087–1095.
22. Vinegoni C, Botnaru I, Aikawa E, Calfon MA, Iwamoto Y, Folco EJ *et al.* Indocyanine green enables near-infrared fluorescence imaging of lipid-rich, inflamed atherosclerotic plaques. *Sci Transl Med* 2011;**3**:84ra45.
23. Joner M, Finn A, Farb A, Mont EK, Kolodgie FD, Ladich E *et al.* Pathology of drug-eluting stents in humans. Delayed healing and late thrombotic risk. *J Am Coll Cardiol* 2006;**48**:193–202.
24. Hara T, Ughi GJ, McCarthy JR, Erdem SS, Mauskapf A, Lyon SC *et al.* Intravascular fibrin molecular imaging improves the detection of unhealed stents assessed by optical coherence tomography *in vivo*. *Eur Heart J* 2015;**12**:ehv677.
25. Bourantas C V, Jaffer FA, Gijsen FJ, Van Soest G, Madden SP, Courtney BK *et al.* Hybrid intravascular imaging: recent advances, technical considerations, and current applications in the study of plaque pathophysiology. *Eur Heart J* 2016;ehw097.
26. Goldstein JA, Maini B, Dixon SR, Brilakis ES, Grines CL, Rizik DG *et al.* Detection of lipid-core plaques by intracoronary near-infrared spectroscopy identifies high risk of periprocedural myocardial infarction. *Circ Cardiovasc Interv* 2011;**4**:429–37.
27. Yoo H, Kim JW, Shishkov M, Namati E, Morse T, Shubochkin R *et al.* Intra-arterial catheter for simultaneous microstructural and molecular imaging *in vivo*. *Nat Med*2011;**17**:1680–4.

28. Jansen K, van der Steen AFW, van Beusekom HMM, Oosterhuis JW, van Soest G. Intravascular photoacoustic imaging of human coronary atherosclerosis. *Opt Lett* 2011;**36**:597–9.
29. Brugaletta S, Garcia-Garcia HM, Serruys PW, De Boer S, Ligthart J, Gomez-Lara J *et al*. NIRS and IVUS for characterization of atherosclerosis in patients undergoing coronary angiography. *JACC Cardiovasc Imaging* 2011;**4**:647–55.
30. Koch M, Ntziachristos V. Advancing surgical vision with fluorescence imaging. *Annu Rev Med* 2016;**67**:153–164.
31. Whitley MJ, Cardona DM, Lazarides AL, Spasojevic I, Ferrer JM, Cahill J *et al*. A mouse-human phase 1 co-clinical trial of a protease-activated fluorescent probe for imaging cancer. *Sci Transl Med* 2016;**8**:320ra4.
32. Nissen SE, Nicholls SJ, Sipahi I, Libby P, Raichlen JS, Ballantyne CM *et al*. Effect of very high-intensity statin therapy on regression of coronary atherosclerosis: the ASTEROID trial. *JAMA Am Med Assoc* 2006;**295**:1556–65.